

Article

Identifying the Groundwater Sources of Huangtupo Landslide in the Three Gorges Reservoir Area of China

Shen Cao ¹, Wei Xiang ^{1,2,*}, Jinge Wang ², Deshan Cui ¹  and Qingbing Liu ² 

¹ Faculty of Engineering, China University of Geosciences, Wuhan 430074, China; caoshen0108@hotmail.com (S.C.)

² Badong National Observation and Research Station of Geohazards, China University of Geosciences, Wuhan 430074, China

* Correspondence: xiangwei@cug.edu.cn

Abstract: Groundwater plays a crucial role in triggering and reactivating deep-seated landslides. However, classical hydrogeological investigations have limitations in their applicability to deep-seated landslides due to anisotropic and heterogeneous media. The Huangtupo landslide in the Three Gorges Reservoir area has garnered significant attention due to its high hazard potential. Of particular interest is the NO.1 Riverside Sliding Mass (HTP-1), which has shown notable deformation and has become the primary focus of landslide research. The study aims to investigate the sources of water in the HTP-1 landslide through hydrochemical analysis. This was achieved by monitoring the major ion content in the groundwater within the landslide for one year. Furthermore, stable isotope investigations were conducted on the groundwater in and around the landslide area, and an analysis of the mineral composition of the landslide soil was also performed. The results indicate that the groundwater in the landslide area (LGW) is a mixture of karst groundwater (KGW) from the adjacent upslope and local precipitation (LP). The karst groundwater is a major contributor to the recharge of the landslide groundwater system, causing a high component of groundwater that can easily exceed the critical level that causes landslide failure during heavy rainfall events. Furthermore, prior to the relocation of residents from the Huangtupo landslide, the landslide groundwater was also impacted by human sewage, which not only affected the chemical composition of groundwater, but also had potential implications for slope stability. These findings provide a more scientific basis for the design and implementation of interception and drainage measures for the Huangtupo landslide and other large-scale landslides with similar geological conditions in the Three Gorges Reservoir area.

Keywords: Huangtupo landslide; groundwater source; hydrochemistry; environmental stable isotopes; Three Gorges Reservoir



Citation: Cao, S.; Xiang, W.; Wang, J.; Cui, D.; Liu, Q. Identifying the Groundwater Sources of Huangtupo Landslide in the Three Gorges Reservoir Area of China. *Water* **2023**, *15*, 1741. <https://doi.org/10.3390/w15091741>

Academic Editors: Zhongjian Zhang, Guoxiang Yang, Mingdong Zang, Feiyong Wang and Gang Mei

Received: 22 March 2023

Revised: 24 April 2023

Accepted: 26 April 2023

Published: 30 April 2023



Copyright: © 2023 by the authors. Licensee MDPI, Basel, Switzerland. This article is an open access article distributed under the terms and conditions of the Creative Commons Attribution (CC BY) license (<https://creativecommons.org/licenses/by/4.0/>).

1. Introduction

Groundwater is known to play a significant role in the triggering and reactivation of deep-seated landslides [1–3]. However, conventional hydrogeological investigations have limitations in their applicability to such landslides, which typically have anisotropic and heterogeneous media [4–8]. The Huangtupo landslide in the Three Gorges Reservoir area is one such landslide that has attracted considerable attention in China due to its large-scale, complex geological structure, and high potential hazard (Figure 1). The recent monitoring data indicate that, among the four parts of the Huangtupo landslide, the deformation speed caused by rainfall in the front area of the NO.1 Riverside Sliding Mass (HTP-1) is about 5mm per month [9], while the overall deformation of the other three landslide masses is relatively small [10]. Therefore, the NO.1 Riverside Sliding Mass has become the focus of landslide research (Figure 1c). Previous studies on the hydrogeology-related inferences of HTP-1 have mostly relied on planar geological surveys and monitoring of borehole water levels, and no targeted research has been conducted to investigate the groundwater source in the landslide [11].

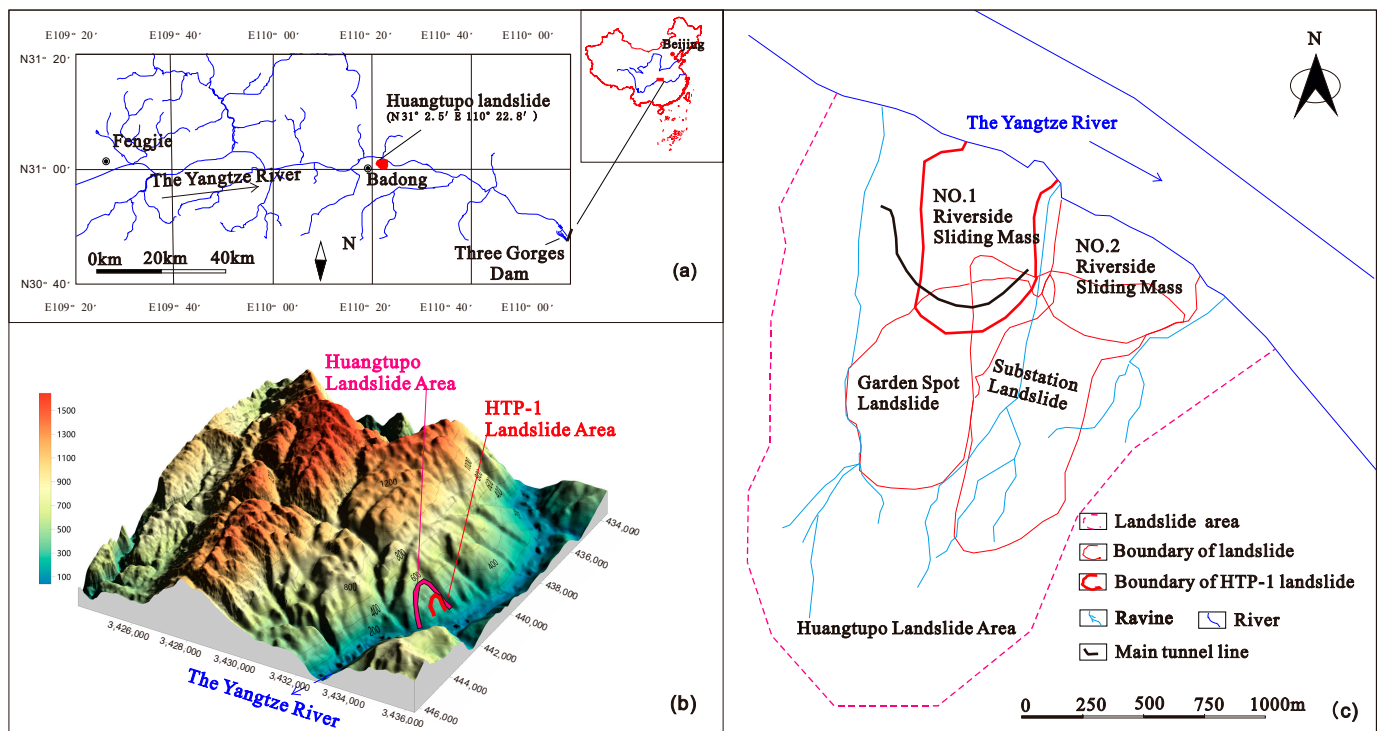


Figure 1. (a) The study area location in Yangtze River. Inset map shows the general location in China. (b) 3D map of study area. (c) Distribution of four parts of the Huangtupo landslide and their respective locations.

Previous studies have suggested that the groundwater source of the Huangtupo landslide is primarily from local precipitation based on its structural and lithological characteristics [9,11–14]. As shown in Figures 2 and 3, the Middle Triassic Badong Formation (T_2b^2), which is composed of weakly permeable sandstone and mudstone layers that are more than 400 m thick, is distributed above the landslide and has traditionally been considered a relatively impermeable layer in previous regional hydrological investigations (Figure 4). Therefore, despite the presence of karstic limestone containing groundwater at the upper part of the slope above the landslide, previous studies on Huangtupo suggested that the karstic water in the upper part of the slope could not replenish the groundwater in the landslide due to being isolated by the sandstone and mudstone layers of the Middle Triassic Badong Formation (T_2b^2) [13]. Instead, the karstic water was thought to flow through the limestone formations on both sides of the landslide and discharge into the Yangtze River, without replenishing the groundwater in the landslide.

Excavation of a 908 m underground test tunnel in the rear part of the HTP-1 landslide in 2012 revealed that the groundwater system of the landslide consistently exhibited rapid and stable recharge characteristics. The significant amount of groundwater that cannot be drained even during the dry season has posed great difficulties for tunnel excavation work. However, the recharge water, in terms of both volume and rate, cannot be solely attributed to local precipitation.

Based on this phenomenon, a hypothesis has been proposed that there is another stable and abundant recharge source for the landslide, in addition to local precipitation, which has caused a high component of groundwater in the HTP-1 landslide, significantly increasing the risk of instability under precipitation conditions. These findings highlight the need for further focused investigation and research.

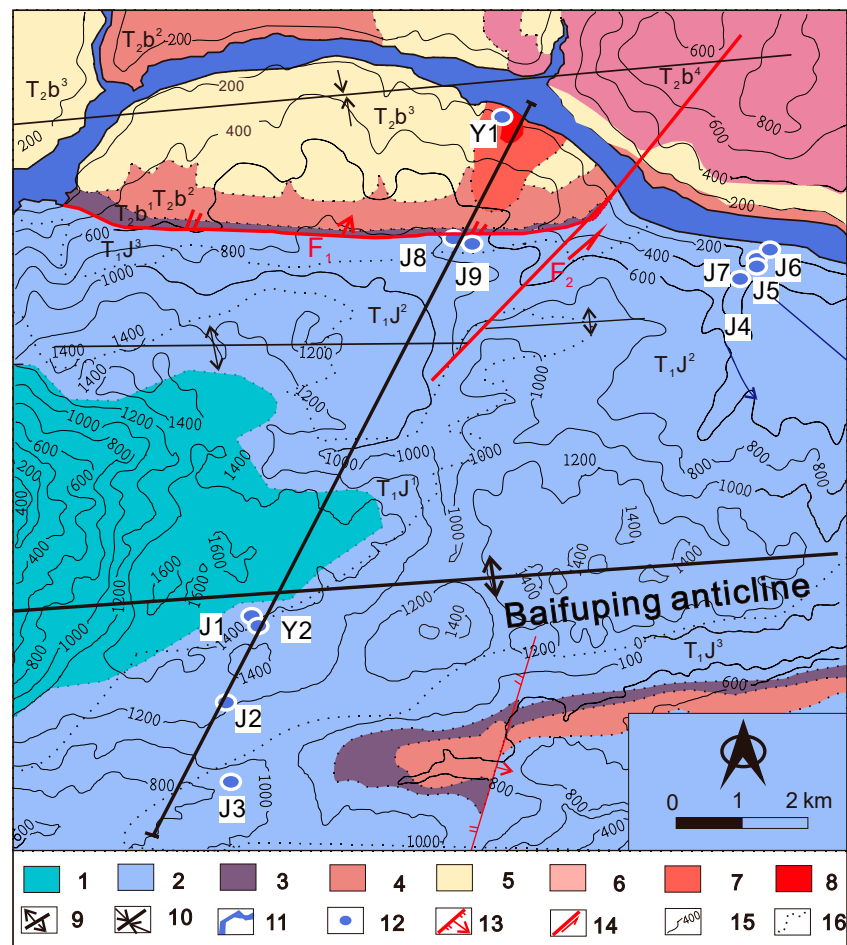


Figure 2. Geological map of study area. Legend: 1. T₁d; 2. T₁j; 3. T₂b¹; 4. T₂b²; 5. T₂b³; 6. T₂b⁴; 7. Huangtupo landslide; 8. HTP-1 landslide; 9. anticline; 10. syncline; 11. water line; 12. sampling point; 13. Badong fault; 14. strike fault; 15. contour line; and 16. stratigraphic boundary.

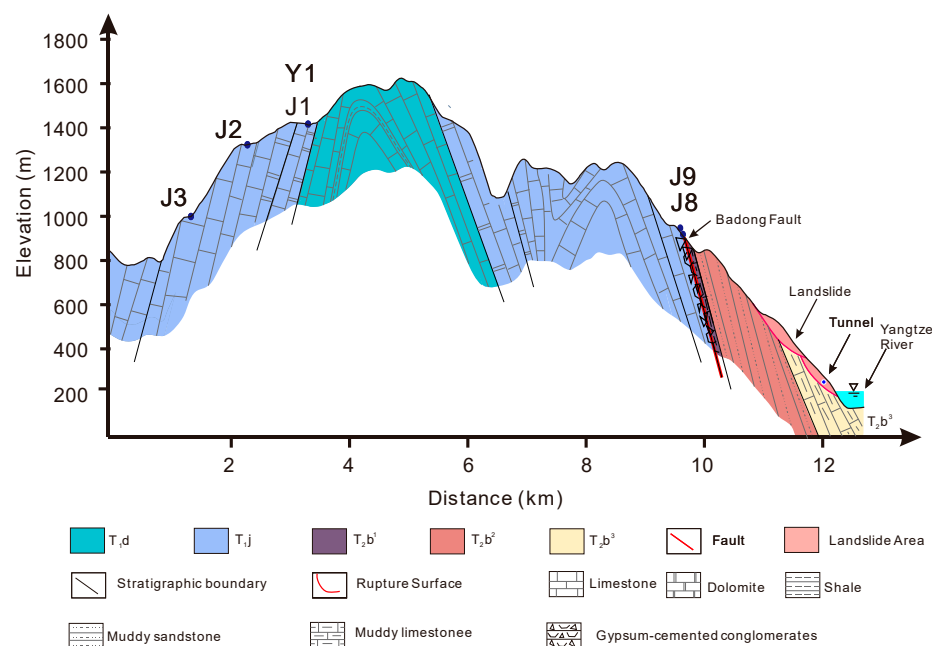


Figure 3. A cross section of the study area.

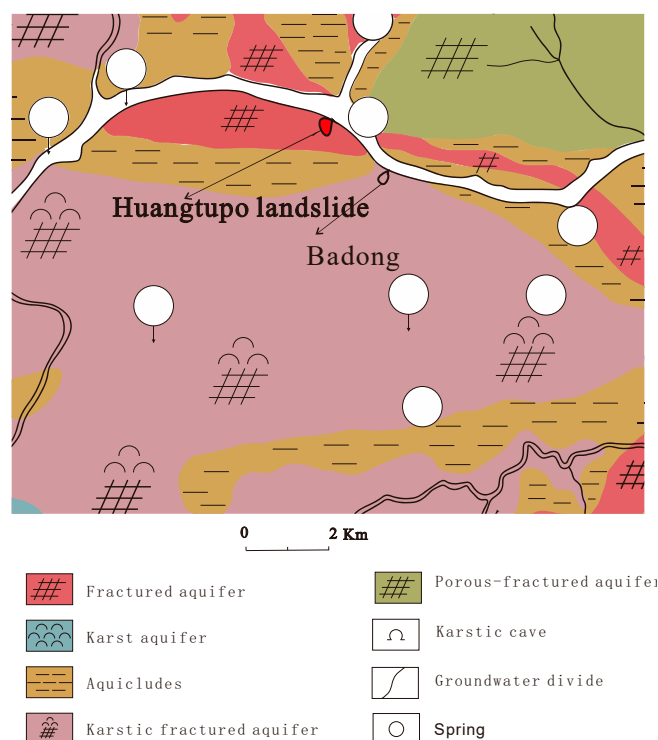


Figure 4. The previous regional hydrogeological map used in previous studies (according to Hubei Geological Bureau, 1977).

Classical hydrogeological investigations are limited in their application to deep-seated landslides due to the anisotropic and heterogeneous nature of the media [4–8]. In recent years, research efforts have focused on indirect methods such as monitoring natural chemical elements, stable isotope tracers, and artificial tracers in groundwater to address this issue.

Analyzing the hydrochemical characteristics of springs on the landslide can identify the source of groundwater and even infer geological information that is not exposed on the surface. In a study by Guglielmi [15] on the Clapière landslide, chemical analyses of springs at different locations revealed significant differences in chemical types between the upper and lower parts of the slope, which could not be explained by internal water–rock interactions. By utilizing hydrogeochemical modeling and geological information, the source of SO_4^{2-} was inferred to be from the underlying and trapped Triassic gypsum rock. Moreover, Guglielmi et al. [16] found that the acceleration period of the landslide and the dilution period of the springs were roughly synchronous, with similar durations. Although there was no linear relationship between the two, this discovery still indicated that a relatively small amount of infiltrating water could trigger the overall acceleration of the La Clapière landslide. Similarly, F. Cervi [17,18] conducted five years of monitoring of groundwater levels and chemical components at the Ca’ Lita landslide in northern Italy. Using isotope tracers and hydrochemical modeling, the study revealed that the primary source of groundwater supply for the landslide was the oil field water crossing the fault zone in the landslide area.

Distinctive isotopic signatures of hydrogen and oxygen in water can be used to differentiate between water formed in different environments [19]. The hydrogen and oxygen isotope compositions in water are not significantly altered by water–rock reactions under normal temperatures [20]. This conservative property of stable isotopes makes them useful tracers for investigating hydrological relationships between different water bodies [21]. Hydrogen and oxygen stable isotopes are natural tracers of water bodies and are commonly used in the field of water resources investigation [4,22,23]. In recent years, these isotopes have been increasingly applied in the study of geological hazards. Compagnon [24] utilized the relationship between elevation and isotope composition

of environmental stable isotopes to determine the elevation of the recharge area for the La Clapière landslide by analyzing the $\delta^{18}\text{O}$ characteristics of springs on the landslide. Guglielmi et al. [15] determined the $\delta^{18}\text{O}$ gradient of the S chilienne landslide by analyzing spring water samples with known recharge area elevations. In addition to using $\delta^{18}\text{O}$, Tsung-Ren Peng [21] also employed tritium to analyze the water samples of landslides and estimate the age of the groundwater. Furthermore, Tsung-Ren Peng [25] utilized environmental stable isotopes to verify that the groundwater sources of a creeping landslide adjacent to a hydropower plant in northern Taiwan included both precipitation and leaks from the plant's water transport system. According to Mebrahtu [26], using converging evidence from geological, geomorphological, geophysical, hydrogeochemical, and isotopic investigations, it was found that shallow-to-intermediate aquifers cause groundwater flow into the landslide mass, thereby influencing its stability.

In addition, artificial tracing techniques have been applied to investigate the groundwater flow pattern and aquifer structure of landslides. Binet et al. [27] studied groundwater flow paths by analyzing natural and artificial chemical tracers in hydrogeological environments. Charlier et al. [28] used continuous measurements of dissolved organic matter fluorescence to characterize the rapid infiltration of an unstable fractured hillside. A. Vallet [29] established a groundwater conceptual model of the S chilienne landslide in western France using isotope tracing experiments, revealing the dual aquifer structure of the landslide. Specifically, there exists a discontinuous and time-varying hidden aquifer in the unstable upper zone, which is mainly recharged by local precipitation through the widely developed fractures within the slope.

Hydrochemical methods provide valuable insights into the hydrogeological conditions of landslides. However, investigations into the sources of groundwater in landslides within the Three Gorges Reservoir area are mostly limited to the landslide area [6,11,30–34], based on traditional methods of geological surveys. The study aims to investigate the sources of water in the HTP-1 landslide through hydrochemical analysis, identifying any additional sources of water beyond precipitation, which can lead to significant improvements in the design of drainage practices in the landslide.

2. Materials and Methods

2.1. Study Area

The study area is located in the Three Gorges Reservoir Area of Badong County, Hubei Province, China (Figure 1a). The area has distinct seasons and abundant precipitation, with an annual average rainfall of 1100.7 mm, mainly concentrated from April to September, accounting for 71.8% of the total annual rainfall.

According to the hydrogeological survey report of Badong sheet (110°00'–111°00' E, 30°40'–31°20' N), the Badong area is divided into eight hydrogeological units and 18 sections based on the tectonic features and topographic characteristics. The study area is located in the Bianlianping hydrogeological unit (VI) and the Baifuping section (Section number 14), as shown in Figure 5. This zone is mainly characterized by the Baifuping anticline, and the hydrological conditions are mainly controlled by the fold structure. From a geomorphological perspective, the carbonate rock formations in the Badong area have formed multi-layer karst landforms through long geological processes under the combined influence of tectonic structures and external forces, namely the five-level denudation surfaces of the western Hubei Mountains. The first denudation surface (S1) at an elevation of 1700–2000 m was formed at the end of the Cretaceous period, the second denudation surface (S2) at an elevation of 1300–1500 m was formed at the end of the early Tertiary period, the third denudation surface (S3) at an elevation of 1000–1200 m was formed during the late Tertiary and early Pleistocene, the fourth denudation surface (S4) at an elevation of 800–900 m was formed during the early Pleistocene, and the fifth denudation surface (S5) at an elevation of 500–700 m was formed at the end of the early Pleistocene. Among them, the first and second denudation surfaces are characterized by surface karst depressions and open valley bottoms, dominated by the development of vertical karst channels, while

the third, fourth, and fifth denudation surfaces are characterized by karst depressions and peaks, dominated by the development of horizontal karst channels. The second-level erosion surface is developed within the study area, as shown in Figure 5, and is the main recharge area for groundwater in the Baifuping section (Figure 5).

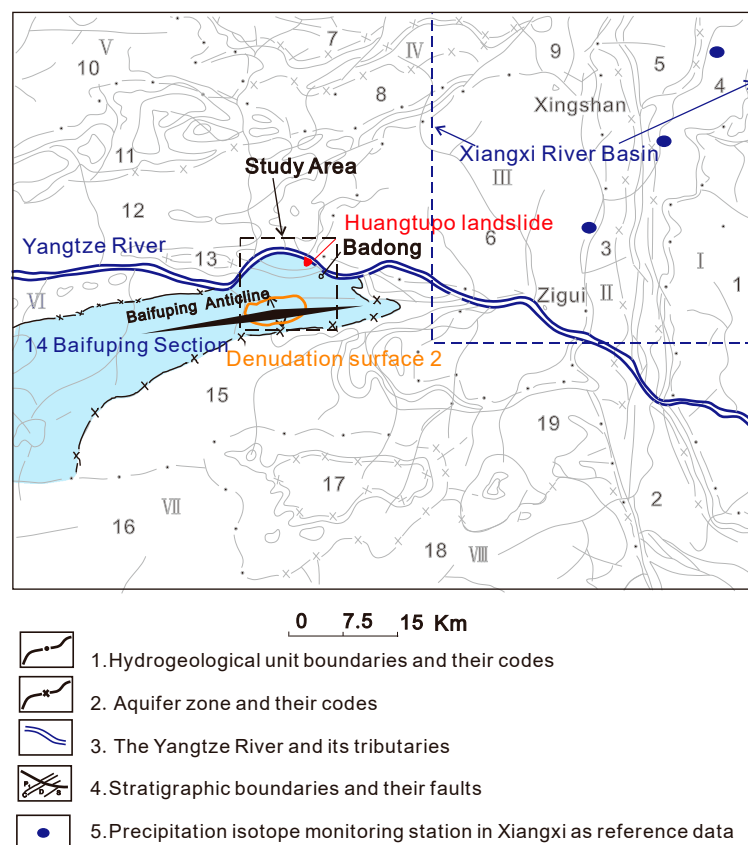


Figure 5. Schematic diagram of hydrogeological unit division in Badong sheet (according to Hubei Geological Bureau, 1977).

The Huangtupo landslide is located on the fan-shaped slope on the south bank of the Yangtze River (Figure 1), with an area of $135 \times 10^4 \text{ m}^2$ and a volume of $6934 \times 10^4 \text{ m}^3$. The sliding surface is up to 100 m below the earth surface, and the sliding mass comprises structurally loose fragmented rocks and block rocks, as well as multiple layers of soft interbedded clay with high content.

The NO.1 Riverside Sliding Mass (HTP-1) is one of the four parts of the Huangtupo landslide. Given its direct contact with the Yangtze River and the periodic fluctuations of the reservoir water level (ranging from 145 m to 175 m), the HTP-1 landslide is the main and most dangerous area of the landslide, making it the primary focus of landslide research.

In this study, the slope where the Huangtupo landslide is located was selected as the research area (Figure 2), and ranges in elevation from the Baifuping syncline axis to the Yangtze River, including the landslide area, the karst area above the landslide area, and the karst area on the east side of the landslide area.

The main lithologies of the study area comprise a succession of sedimentary rocks belonging to the Upper Triassic Badong Formation and Lower Permian Jialingjiang Formation and Daye Formation. The Badong Formation consists of three sections (T_2b^1 , T_2b^2 , and T_2b^3) that exhibit varying lithologies. The first and third sections of the formation are primarily composed of muddy limestone, and are mainly carbonate rocks and developed with structural fractures and dissolution fractures, while the second section consists of interbedded sandstone and mudstone. In contrast, the Jialingjiang Formation (T_1j) is mainly composed of limestone and dolomite, while the Daye Formation (T_1d) is characterized

by the presence of micritic limestone and shale. Of particular note, gypsum-cemented conglomerates are developed near the contact zone between the Badong Formation and the Jialing River Formation.

2.2. Samples

The Three Gorges Research Center for Geohazards (TGRC) of the China University of Geosciences (CUG), supported by the China Ministry of Education, have built a large field test site in the Huangtupo landslide to provide an unprecedented opportunity to research reservoir landslides. A group of tunnels with a total length of 1.1 km has been constructed in the HTP-1 landslide, and, additionally, nine boreholes, with a cumulative length of 894 m, have been drilled into the sliding mass [11]. The main tunnel traverses the sliding bed, sliding zone, and sliding mass of the landslide from west to east. The third and fifth branch tunnels (BR3, BR5) have been excavated from south to north to expose the sliding zone (Figure 6). This experimental site provides excellent conditions for sampling groundwater, particularly fresh groundwater near the sliding rupture zone, at various locations within the landslide.

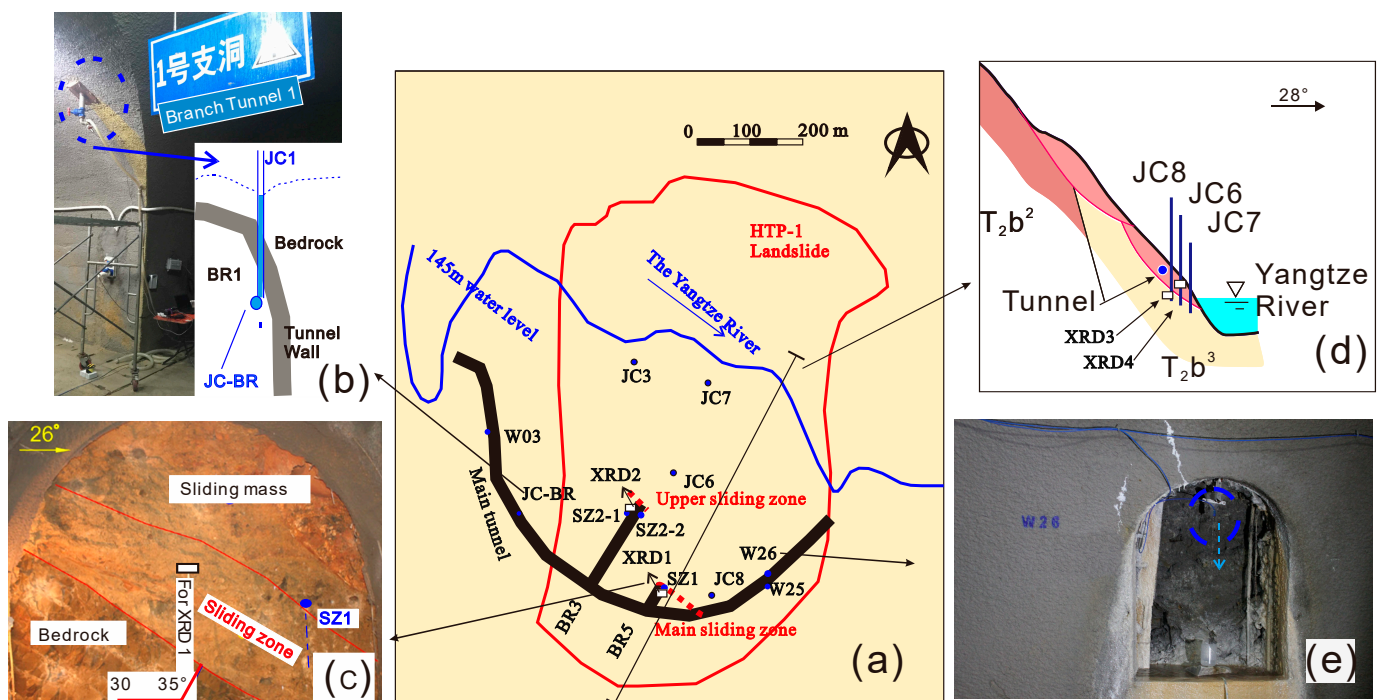


Figure 6. (a) Sampling locations of landslide area. (b) Photo and schematic of the sampling environment for sample JC-BR. (c) Photograph of the sampling environment for samples SZ1 and XRD-1 at the sliding surface. (d) A profile view showing the location of boreholes and tunnels, as well as the positions of samples XRD-3 and XRD-4. (e) Photograph of the sampling environment for the water sampling window on the tunnel wall (using W26 as an example).

From January 2015 to January 2016, a year-long hydrochemical monitoring was conducted at five points in the tunnel, with groundwater sampling and hydrochemical analysis performed approximately once a month. Specifically, W03, W25, and W26 were sampled from groundwater exposure points reserved on the side wall of the underground tunnel, while SZ1 and SZ2-1 were sampled from the tunnel faces that expose the sliding zone. W03 is located on the bedrock of the landslide in the west section of the tunnel, while W25 and W26 are located on the sliding mass in the east section of the tunnel. SZ2-1 is located on the upper sliding fracture surface exposed in the third branch tunnel, while SZ1 is located on the main sliding fracture surface exposed in the fifth branch tunnel (Figure 6).

To exclude the potential influence of domestic wastewater from residents on the ground-water stable isotope content at the landslide site, stable isotope investigations were conducted in 2016 after the completion of the resettlement work on Huangtupo. In addition, it should be noted that, during high water levels in the Three Gorges Reservoir, the river level may rise too quickly, exceeding the rate of groundwater level rise at the front edge of the landslide, resulting in brief backflow of reservoir water to supplement groundwater at the front edge of the landslide. This adds complexity to the analysis of groundwater sources. Therefore, we chose August in 2016, when the reservoir water level was at its lowest (145.03 m), to collect stable isotope samples of groundwater, surface water, and precipitation. All samples were collected within four days to ensure the effectiveness of the analysis.

During the stable isotope sampling campaign, a total of 22 samples were collected, including 2 precipitation samples (Y1 and Y2), 9 samples from the karst area (Figures 2 and 3), and 11 samples from the landslide area (Figure 6). The precipitation samples were collected from different elevations in the study area to verify the applicability of the stable isotope characteristics of regional atmospheric precipitation in the study area. Among the samples from the karst area, J8 and J9 were surface water samples, and the rest were groundwater samples from different elevations. J8 was collected from a natural small lake, while J9 was sampled from an artificial pond constructed by farmers to collect water from the mountain for irrigation purposes. Samples J1–J3 and J7 were obtained from springs at different elevations, while samples J4–J6 were collected from outlets of the underground river that drains into the Yangtze River from karst water systems. The number of sample points in the landslide area increased to 11, with JC3, JC7, JC6, and JC8 obtained from boreholes, and BR-JC from the bottom of drainage borehole JC1 and the top of the tunnel BR1 (see Figure 3). The drainage borehole JC1 was drilled downwards from the slope surface and intersected with the tunnel BR1, forming a three-dimensional drainage system that combined vertical boreholes and horizontal tunnels.

Clean polyester bottles were used for sample collection of precipitation, surface water, and groundwater in the study area. Prior to fieldwork, bottles were washed with distilled water three times to remove dust and then air-dried. In the field, the bottles were rinsed on site with a large volume of the sample water to be measured, for 3–4 times before sampling.

During the sampling process, it was ensured that there were no bubbles in the bottles to avoid chemical reactions between the air and samples during storage, which could affect the accuracy of the data. After sampling, the water was quickly filtered, sealed with paraffin film, and stored at a low temperature. In particular, samples for cation analysis were acidified to $\text{pH} < 2$ with 98.6% HNO_3 at the sampling site.

Rock and soil samples from the landslide were collected and analyzed for their mineral composition. The stratigraphic sequence of the landslide area is stable and mainly composed of muddy limestone formations, as well as soft interlayered clayey silt and sliding zones that have formed due to the evolution of soft interlayers [35]. To obtain a representative sample set, four samples were collected from drilling and tunneling locations: XRD1 (clayey silt at the main sliding zone), XRD2 (clayey silt at the upper sliding zone), XRD3 (strongly karstified muddy limestone), and XRD4 (soft interlayered clayey silt).

2.3. Analyses

Cations were analyzed using inductively coupled plasma optical emission spectrometry (ICP-OES) with an iCAP6300 instrument, achieving an analytical precision of 0.001 mg/L. Anion analysis was carried out with an ion chromatography system (ICS-2100), achieving an analytical precision of 0.001 mg/L. HCO_3^- was analyzed using an acid–base titration method on the day of field sampling. The total relative uncertainty was less than 5% for all compounds.

The stable isotope analysis was conducted using an IWA-35-EP liquid water stable isotope analyzer from LGR (Los Gatos Research), USA. This instrument utilizes the Beer–Lambert law and off-axis integrated cavity output spectroscopy (OA-ICOS) technology, which enables simultaneous measurement of δD and $\delta^{18}\text{O}$ compositions in water. The testing error

for δD is $\pm 0.6\text{‰}$ and for $\delta^{18}O$ is $\pm 0.2\text{‰}$. Before the samples were tested, they were filtered through a $0.22\ \mu\text{m}$ syringe filter to remove any interference from particles in the water. The testing temperature was 26°C , and the testing results are expressed in ‰ deviation values relative to V-SMOW (Vienna Standard Mean Ocean Water). Deuterium excess values were calculated according to Dansgaard (1964) as $d = \delta D - 8 \cdot \delta^{18}O$. (Tables 1 and 2).

Table 1. Stable oxygen and hydrogen isotopic compositions for precipitation, surface water, and groundwater in karst area.

Samples	Precipitation				Groundwater					Surface Water	
	Y1	Y2	J1	J2	J3	J4	J5	J6	J7	J8	J9
Elevation(m)	276	1589	1500	1249	905	301	285	192	219	812	815
$\delta D\ \text{‰}$	−27.5	−56.1	−54.2	−54.2	−52	−54.9	−54.7	−56.1	−54.8	−47.2	−44.4
$\delta^{18}O\ \text{‰}$	−5.2	−8.6	−8.5	−8.5	−8.3	−8.5	−8.6	−8.5	−8.6	−6.1	−6
$d\ \text{‰}$	14.1	12.7	13.8	13.8	14.4	13.1	14.1	11.9	14	1.6	3.6

Table 2. Stable oxygen and hydrogen isotopic compositions for groundwater in landslide area.

Samples	JC3	JC7	JC6	JC8	W26	W25	W03	SZ1	SZ2-1	SZ2-2	JC-BR
Z*/m	142	143	162.8	195.6	190	190	180	185	185	185	180
Z/m	183.5	176.3	209.8	263.6	250	235	230	225	275	275	263.5
$\delta D\ \text{‰}$	−53	−54.4	−53.4	−50.1	−52.1	−53	−54.4	−49.1	−46.2	−44.7	−49
$\delta^{18}O\ \text{‰}$	−8.1	−8.2	−8.2	−8.2	−7.9	−8.3	−8.3	−7.5	−7.3	−7.2	−7.5
$d\ \text{‰}$	11.8	11.2	12.2	13.1	13.5	13.4	12	10.9	12.2	12.9	11

Note: Z* represents the elevation of the sampling point; and Z represents the corresponding slope surface elevation vertically above the sampling point.

Two major rupture zones were sampled in BR-3 at K3 + 138 m and in BR-5 at K5 + 21.7 m, together with soil and rock samples obtained from two boreholes, and their mineral composition and content were analyzed using X-ray diffraction analysis. The details of sampling locations and the XRD analysis results are shown in Table 3.

Table 3. Mineral composition table of landslide soils and rocks.

Samples	Location	Description	Relative Mineral Content (%)						
			Quartz	Feldspar	Calcite	Montmorillonite	Chlorite	Illite	Kaolinite
XRD1	K5 + 21.7 m	clayey silt at main sliding zone	28	2	22	18	8	22	0
XRD2	K3 + 138 m	clayey silt at upper sliding zone	23	4	32	13	6	22	0
XRD3	JC8 – 112 m	strongly karstified muddy limestone	11	6	43	1	6	27	6
XRD4	JC6 – 35.3 m	soft interlayered clayey silt	14	6	40	10	5	25	0

2.4. Definition of Reference Isotopic Values for Precipitation

2.4.1. LWML in Study Area

The isotopic composition of deuterium and oxygen in precipitation exhibits a linear relationship, known as the meteoric water line (MWL) [36]. Due to the influence of local climate factors, such as the origin of water vapor, secondary evaporation during precipitation events, and seasonal variations in precipitation, local meteoric water lines differ among regions. In 1961, Craig [36] proposed the global meteoric water line (GMWL): $\delta D = 8 \delta^{18}O + 10$. Subsequently, observations of hydrogen and oxygen isotopes in precipitation were carried out in different regions. Zheng et al. derived the MWL for China

(CMWL) using 107 precipitation data: $\delta D = 7.9 \delta^{18}O + 8.2$ [37]. Zhao Jiacheng established the MWL in the Yichang area, which is located 63 km away from the Huangtupo landslide, as follows: $\delta D = 8.4 \delta^{18}O + 15$ ($r = 0.977$). In 2016, Huang et al. conducted a study in the Xiangxi River basin, which is located 39 km away from the Huangtupo landslide (Figure 5), and established the MWL as $\delta D = 8.17 \delta^{18}O + 13.38$ ($r = 0.995$) [38]. It can be observed from Figure 7 that these two GMWLs are very close to each other.

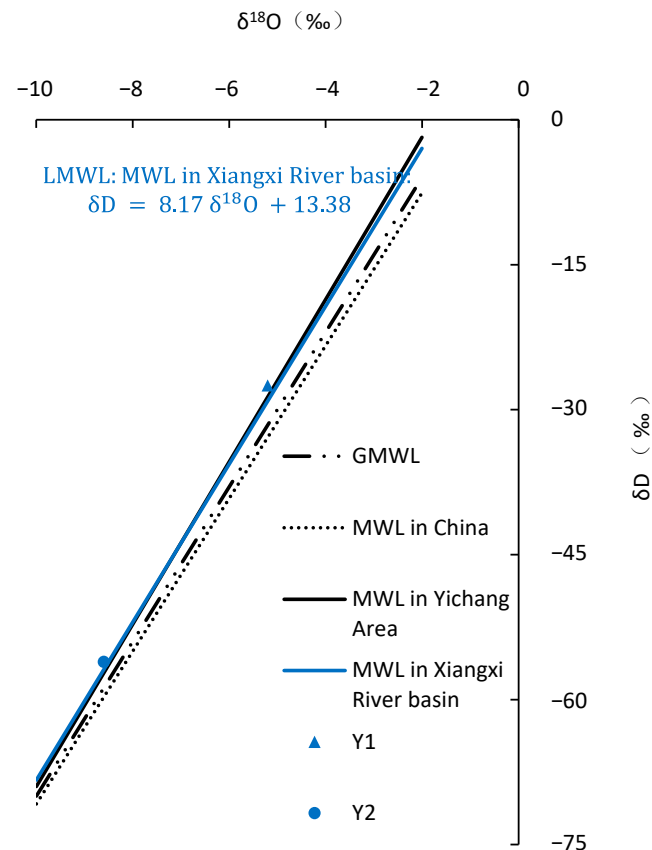


Figure 7. Plot of δD versus $\delta^{18}O$ of measured precipitation. Meteoric water lines (WMLs) in global area, China Area, Yichang Area, and Xiangxi Area.

In Figure 7, the stable isotopic data of precipitation in the study area are distributed along the meteoric water lines of Yichang and the Xiangxi River basin. Thus, the meteoric water line in Xiangxi River basin, which is closer to Badong, was selected as the local meteoric water line (LMWL), expressed as:

$$\delta D = 8.17\delta^{18}O + 13.38; \quad (1)$$

$N = 92 \quad R = 0.995.$

2.4.2. Altitude Effect of Precipitation in Study Area

Different positions of precipitation exhibit a decrease in δD and $\delta^{18}O$ values with increasing terrain elevation, which is referred to as the altitude effect and typically exhibits a linear relationship [19]. Stable isotope values in high-elevation regions are generally relatively lighter than those in low-elevation regions. This altitude effect is commonly applied to analyze the recharge elevation of groundwater. Yu [39,40] investigated the altitude effect of stable isotope compositions in precipitation in the Sichuan, Guizhou, and Tibet regions of China, and obtained a $\delta^{18}O$ altitude gradient of $-0.26\text{‰}/100 \text{ m}$. Huang et al. conducted a year-long hydrological monitoring of precipitation in the Xiangxi River basin [38], located 39 km from Badong (Figure 5), and obtained a $\delta^{18}O$ altitude gradient of $-0.26\text{‰}/100 \text{ m}$ based on isotopic data from 92 samples. In this study, a height gradient

value of $-0.26\text{‰}/100\text{ m}$ was calculated based on precipitation samples collected at different elevations (Table 1), which is consistent with the reference value in the literature and further supports the applicability of using this gradient in the study.

Based on the altitude gradient and isotopic values of measured precipitation on the landslide, the mathematical regression between the $\delta^{18}\text{O}$ value and altitude can be expressed as follows:

$$\delta^{18}\text{O} = -2.6 \times 10^{-3}Z - 4.48 \quad (2)$$

where $\delta^{18}\text{O}$ represents the oxygen isotope composition of precipitation at a given elevation Z , and Z is in meters (EL).

2.5. Isotopic Equation for Mixed Water Samples

The use of stable isotopes allows for the determination of the mixing ratio of mixed water samples [17,21,25,41]. When groundwater is formed by mixing N different sources, the mixing ratio of oxygen isotopes in the resulting groundwater can be expressed using the following equation:

$$\delta_{\text{mix}} = \sum(f_i \times \delta_i) \quad (3)$$

Here, δ_{mix} is the oxygen isotope composition (‰) of the mixed groundwater, δ_i is the oxygen isotope composition (‰) of the i -th source groundwater, and f_i is the mixing ratio of the i -th source groundwater. The summation is taken over all N sources of groundwater.

3. Results and Discussion

3.1. Groundwater Chemical Analyses and the Source of LGW

Water chemistry monitoring for one year showed that the pH of the groundwater samples in the landslide area ranged from 7.25 to 8, with electrical conductivity between 320 and 686 $\mu\text{S}/\text{cm}$. The concentration of HCO_3^- ranged from 64 to 268 mg/L, Cl^- concentration ranged from 11.74 to 41.11 mg/L, NO_3^- concentration ranged from 5.32 to 82.58 mg/L, SO_4^{2-} concentration ranged from 62.11 to 120.34 mg/L, Ca^{2+} concentration ranged from 52.02 to 121.30 mg/L, K^+ concentration ranged from 0.41 to 5.73 mg/L, Mg^{2+} concentration ranged from 1.65 to 5.64 mg/L, and Na^+ concentration ranged from 8.22 to 26.28 mg/L. The water chemistry test results were analyzed using a Piper trilinear diagram, as shown in Figure 8. The main hydrochemical types of LGW were determined to be $\text{HCO}_3\text{-SO}_4\text{-Ca}$ and $\text{SO}_4\text{-HCO}_3\text{-Ca}$ types according to the Schukalev classification method (SCM).

The Piper diagram analysis of the water chemistry testing results did not consider the NO_3^- , which is a typical indicator ion of pollution and is usually derived from human activities. Due to the huge potential for catastrophic landslides on the Huangtupo landslide, the entire town of approximately 20,000 people began to migrate to the west side of the slope from 1992 onwards. The cost of the town relocation was enormous, and it was not until July 2015 that the last batch of residents on the Huangtupo landslide completed their evacuation. As can be seen from Figure 9a, the NO_3^- concentration in the groundwater of the landslide area has significantly decreased since August 2015, which is consistent with the changes in human activities. In January 2016, the NO_3^- concentration in groundwater at each site ranged from 11.76 mg/L to 5.32 mg/L. Compared with January of the previous year (when the concentration range of sulfate ions at each site was 76.72 mg/L to 18.76 mg/L), this significant decrease indicates that the NO_3^- ion in the groundwater comes entirely from the residents' daily life on the landslide.

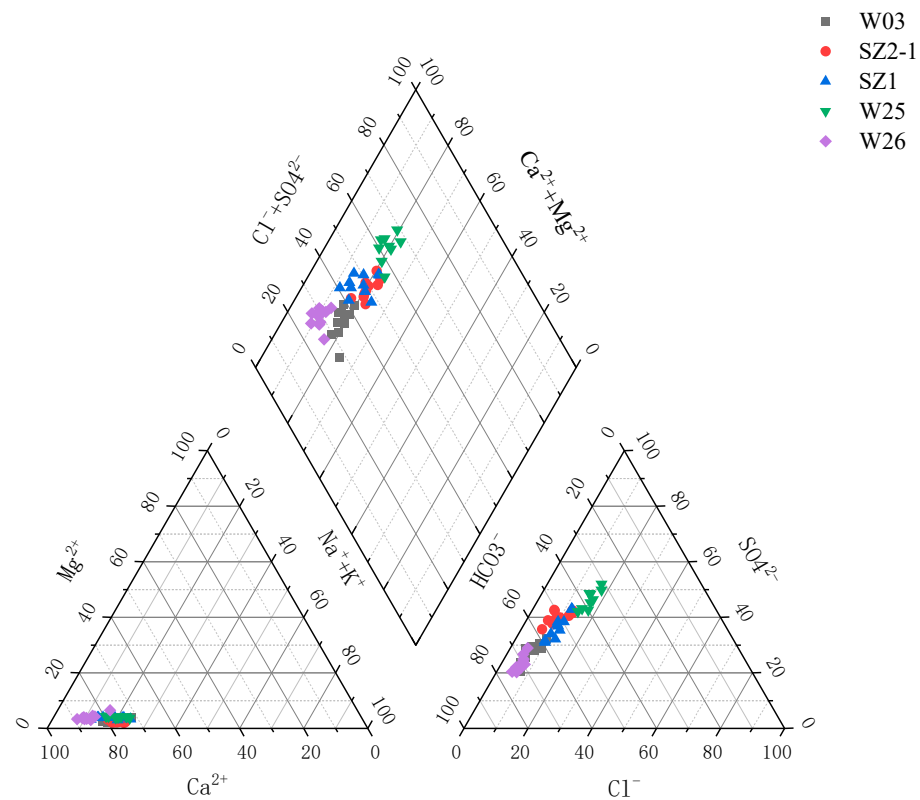


Figure 8. Representation of the composition of the LGW in a Piper diagram.

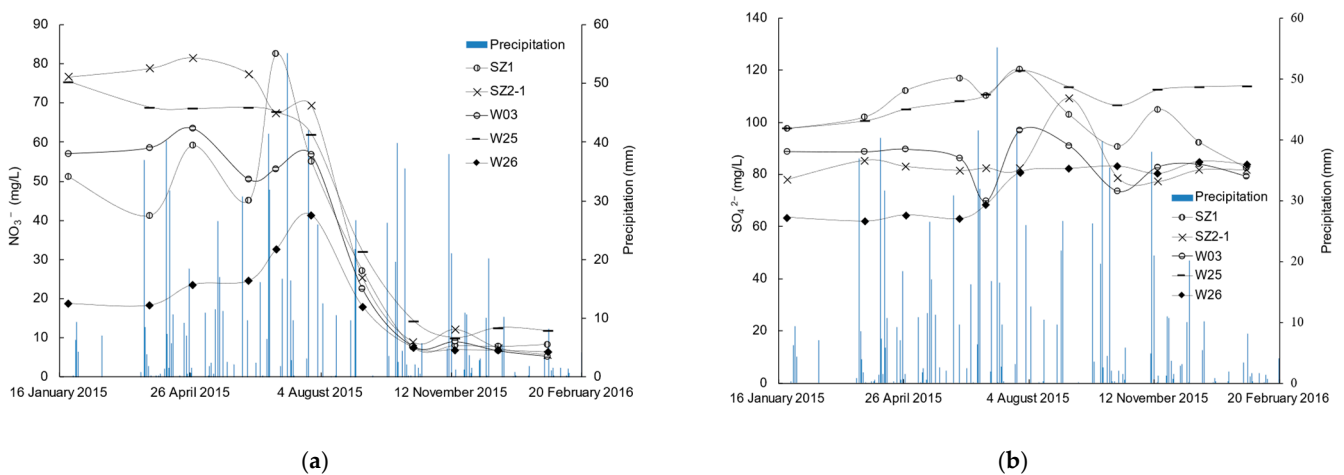


Figure 9. Nitrate ion content (a) and sulfate ion content (b) of groundwater samples from the landslide area.

According to previous survey reports on the Huangtupo landslide, there was no specialized sewage disposal pipeline during the construction of the old village on the landslide. Villagers dumped their household wastewater directly into a natural gully near their houses based on their living habits. This explains the high concentration of nitrate ions in the groundwater before relocation, indicating that a large amount of wastewater from human activities was discharged into the natural gully without bottom treatment, which would supply the groundwater of the landslide. This not only affects the chemical composition of groundwater but also poses a potential threat to the stability of the landslide. This provides a preventive approach for the prevention and control of other ancient landslides coexisting with villages and towns in the Three Gorges Reservoir area. It is necessary to carry out specialized planning for the management of domestic wastewater in villages and towns, in

order to avoid long-term supply of domestic wastewater to the groundwater, which may trigger the reactivation and instability of ancient landslides.

The analysis results show that the dominant cation in the groundwater of the landslide area is calcium ion, which is consistent with the fact that the main lithology in the area is carbonate rocks. The dominant anions are HCO_3^- and SO_4^{2-} , and the concentration of sulfate ions is unusually high. As shown in Figure 9b, the concentration of sulfate ions did not show significant changes throughout the year, which excludes the possibility of short-term accidental or human activity pollution. The samples from W25 (groundwater from the slip zone), SZ1 (groundwater from the main sliding rupture zone), and SZ2-1 (groundwater from the upper sliding rupture zone) had the highest concentration of sulfate ions, exceeding 120 mg/L, followed by W03 (groundwater from the slip zone) and W26 (groundwater from the sliding body). Although the sulfate ion concentration in these samples was relatively low compared with other samples, it was still higher than 62.11 mg/L. Unlike nitrate ions, the sulfate ion concentration did not increase significantly during the rainy season (from April to July 2015) before the residents had completely evacuated, and even showed a certain degree of decrease in SZ1 and W03. The increase in sulfate ion concentration occurred four months after the onset of precipitation, showing a significant lag effect. This indicates that sulfate ions are not derived from local minerals.

After converting the results of chemical analysis testing to milliequivalents, the ion relationships were analyzed. The relationship between $\text{Ca}^{2+} + \text{Mg}^{2+}$ and HCO_3^- is shown in Figure 10, falling to the right of the 1:1 line, indicating that the source of Ca^{2+} and Mg^{2+} is not only from carbonate dissolution. The relationship between $\text{Ca}^{2+} + \text{Mg}^{2+}$ and $\text{HCO}_3^- + \text{SO}_4^{2-}$ is shown in Figure 10b, and the data are evenly distributed on both sides of the 1:1 line, indicating that the chemical composition of Ca^{2+} and Mg^{2+} is mainly produced by the weathering of carbonate and sulfate.

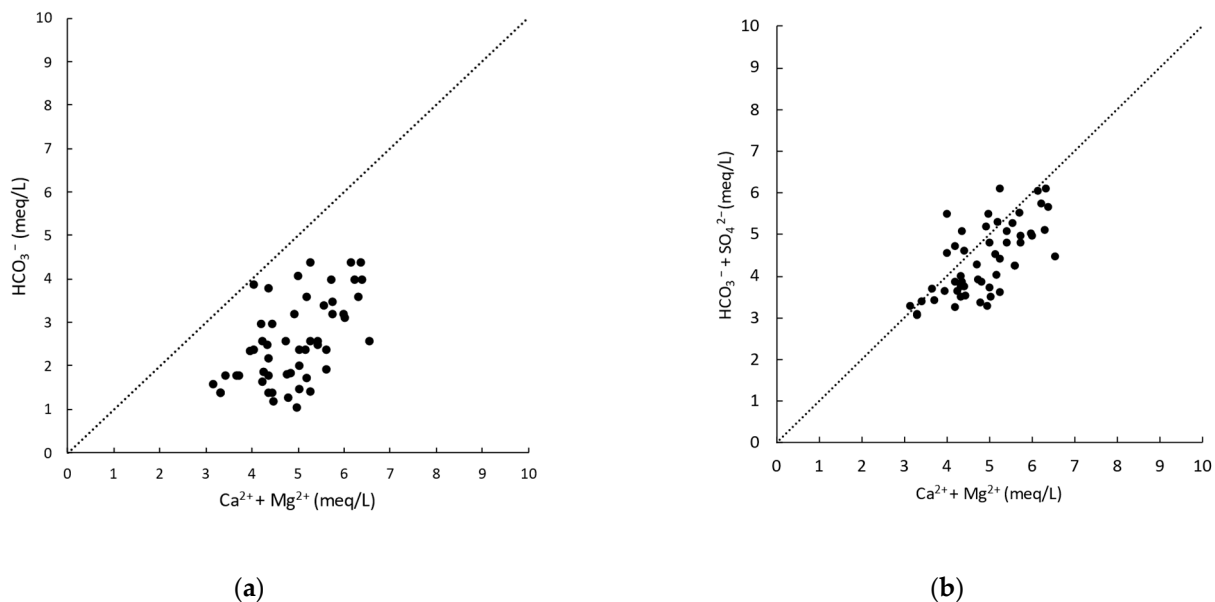


Figure 10. Ion relationship diagram. (a) HCO_3^- vs. $(\text{Ca}^{2+} + \text{Mg}^{2+})$, and (b) $(\text{HCO}_3^- + \text{SO}_4^{2-})$ vs. $(\text{Ca}^{2+} + \text{Mg}^{2+})$.

Mineral analysis results are shown in Table 3, indicating that the mineral composition in the landslide area consists of calcite, quartz, montmorillonite, chlorite, illite, and kaolinite. There are no minerals that could provide sulfate ions. According to regional mineral reports, the gypsum layer in the study area is mainly distributed near the contact surface of the Jialingjiang Formation and the Badong Formation, with a thickness of about 28.5 m. This is the most likely source of sulfate in the nearby area. Based on this, it is

inferred that the groundwater in the landslide area is supplied by karst water from the Jialingjiang Formation.

3.2. Groundwater Isotopic Analyses and the Source of LGW

In this study, the relationship between δD and $\delta^{18}O$ of each sample is shown in Figure 11, and the regression line representing the local meteoric water line (LMWL) is $\delta D = 8.17 \delta^{18}O + 13.38$. As shown in Figure 11, surface water samples, J8 from the lake and J9 from the pond, significantly deviated from the local meteoric water line, which may be due to evaporation or mixing with other surface runoff. The isotopic data of groundwater are distributed on the LMWL, indicating that the groundwater originates from precipitation, and the stable isotopes of the groundwater have not been significantly affected by surface water, water–rock interaction, or evaporation.

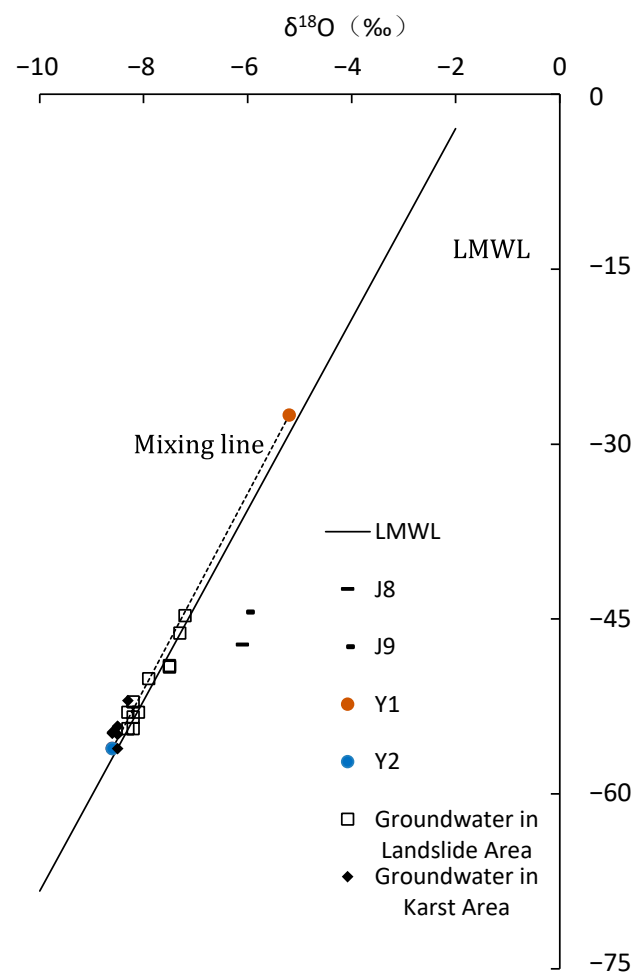


Figure 11. Plot of δD versus $\delta^{18}O$ of measured groundwater, surface water. Meteoric water lines in Xiangxi area as LMWL.

Analysis of the d-excess values of groundwater was conducted to study the impact of seasonal precipitation on groundwater in the region. The d values of precipitation in the area showed a characteristic of being low in the summer and high in the winter, with average values of 10.87‰ and 15.67‰, respectively [38]. Stable isotope sampling was conducted in August, and the d values of karst groundwater ranged from 11.9‰ to 14.40‰, with an average of 13.59‰, while those of groundwater in the landslide area ranged from 11.00‰ to 14.20‰, with an average of 12.27‰. The average d-excess values of groundwater in both areas are higher than the mean value of winter precipitation in the region, but lower than that of summer precipitation. The d-excess value of karst groundwater is higher and

more similar to the d-excess value of summer precipitation in the region. This indicates that groundwater in both areas in August is a mixture of winter and summer precipitation, with a higher contribution from winter precipitation in karst groundwater.

3.2.1. Source of Karst Groundwater (KGW)

Seven groundwater samples in karst regions were collected at elevations ranging from 192 to 1400 m (Figure 2). The stable isotope composition of $\delta^{18}\text{O}$ in these samples remained stable between -8.3‰ and -8.6‰ (Table 1). It is worth noting that the sampling sites of J4, J5, and J6 are located at the outlets of underground rivers deep in the karst riverside slope, where groundwater directly discharges into the Yangtze River. Sample J7 comes from a drainage hole in the deep mountainside along the Yangtze River. These four samples are all located in the discharge area of the karst groundwater system, and their stable isotope $\delta^{18}\text{O}$ values (-8.5‰ ~ -8.6‰) are still the same as the $\delta^{18}\text{O}$ value of the sample at the top of the slope at an elevation of 1500 m (-8.5‰). Considering the measurement error range of the laser isotope analysis instrument of $\pm 0.2\text{‰}$, it can be assumed that the entire karst region has a relatively uniform recharge source. Based on Formula (2), the theoretical elevation of the recharge area was calculated to be between 1489 and 1584 m.

According to the regional tectonic background and geomorphic observation data, a second-level denudation surface (S2) with an elevation range of 1300–1500 m exists in the study area (Figure 5), which is consistent with the calculated theoretical elevation range of the karst water supply area. The consistency of the calculated value with the objective geological conditions further supports the applicability of Formula (2) for estimating the water source in the study area.

3.2.2. Source of Landslide Groundwater (LGW)

Surface surveys show that the elevation range of the outcrop of the third section of the Badong Formation in the landslide area is 330–145 m. According to Formula (2), the theoretical range of stable isotope $\delta^{18}\text{O}$ values of precipitation in the landslide area is calculated to be -5.3‰ to -4.9‰ (Table 2). The measured isotopic $\delta^{18}\text{O}$ value of precipitation at 276 m elevation in the landslide area is -5.2‰ , consistent with the theoretical range. However, the measured range of $\delta^{18}\text{O}$ in the landslide groundwater is -7.2‰ to -8.4‰ , which is much lower than the stable isotope content of local precipitation. This indicates that the landslide groundwater requires lighter $\delta^{18}\text{O}$ sources from higher-altitude precipitation to mix with the local precipitation. Moreover, as previously discussed, surface runoff from the slope can be excluded as a potential source. Consequently, the potential of surface runoff transporting precipitation from higher elevations to the landslide area can also be dismissed. Therefore, it can be inferred that supplies from higher elevations can only enter the landslide groundwater system through subsurface flow. Therefore, it is inferred that karst groundwater is another source of the landslide groundwater.

Eleven LGW data points in Figure 11 are distributed on the mixing line of KGW (karst groundwater) data points and Y1 (precipitation on landslide) measured data points. This indicates that the landslide groundwater (LGW) is a mixture of karst water (KGW) from the upper slope and local precipitation (LP) in the landslide area. This is consistent with the conclusion obtained from the analysis of the main ion relationships: KGW flows through the contact zone between the Jialingjiang Formation and the Badong Formation, which is characterized by a thickness of about 28.5 m of gypsum-cemented conglomerates. The flow rate of the water is slowed down due to the relatively low permeability of the rock layers, and water–rock interactions lead to the dissolution of gypsum, resulting in high concentrations of sulfate ions in the groundwater.

After summarizing previous research reports on the development of structural planes in the second section of the Badong Formation in the study area, it was found that, although the formation is composed of relatively low-permeability fine sandstone, conjugate joints are significantly developed due to strong regional tectonic stress. For example, NE and NW conjugate joints were observed in the T₂b² formation at the eastern end of the old Badong

County to Jiangbeitaizi corner, with the widest crack width reaching 1 m [13]. Therefore, these conjugate joints can serve as good underground water flow channels, providing the possibility for the deep migration of karst water.

According to the above conclusions, the conceptual flow model in the study area is shown in Figure 12.

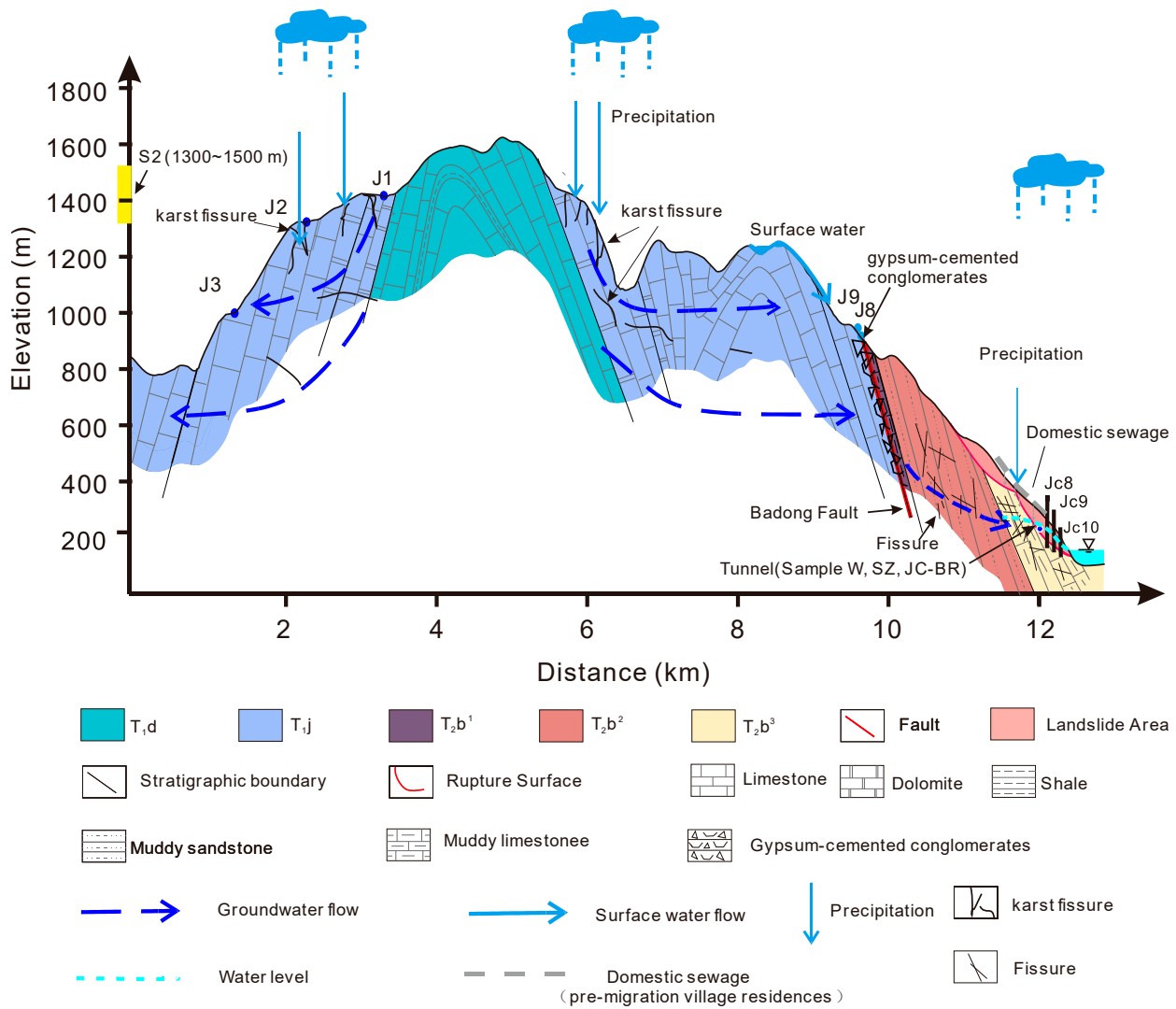


Figure 12. Conceptual flow model in the study area.

3.3. The Source Fraction and Significance of Local Precipitation

According to Formula (3), it is possible to estimate the relative contributions of karst water and local precipitation to the landslide groundwater and can be achieved using a regular two-end member mass balance equation [21,41], where X and (1 - X) are the fractions of LP and KGW in LGW, respectively

$$\delta^{18}O_{LGW} = X \delta^{18}O_{LP} + (1 - X) \delta^{18}O_{KGW} \quad (4)$$

According to Section 3.2.1, the $\delta^{18}O$ values of all karst groundwater in the study area are within the range of $-8.5 \pm 0.2\%$. Since the measurement error range of the laser isotope analyzer is $\pm 0.2\%$, it can be considered that the karst groundwater in the study area has a consistent isotopic composition. The average $\delta^{18}O$ value of seven karst groundwater samples (J1–J7) was calculated as -8.5% . According to Section 3.2.2, the maximum elevation of the outcrop of the third section of the Badong Formation and the

landslide deposits in the landslide area is 330 m, which determines the stable isotope content lower limit of local precipitation in the landslide area as -5.3% . According to Equation (2), the maximum $\delta^{18}\text{O}$ value of the LP in LGW at the slope elevation Z can be calculated.

Based on Formula (4) and the maximum and minimum $\delta^{18}\text{O}$ values of LP recharge, the proportion of LP recharge in each landslide groundwater can be estimated (Table 4).

Table 4. Fractions of respective end sources contribute to groundwater in the studied landslide.

Samples	$\delta^{18}\text{O}(\text{‰})$	Relative Contributing Fraction
JC3	-8.1	$\delta^{18}\text{O} = (88 \pm 1)\% \delta^{18}\text{O}_{\text{KGW}} + (12 \pm 1)\% \delta^{18}\text{O}_{\text{LP}}$
JC7	-8.2	$\delta^{18}\text{O} = (92 \pm 1)\% \delta^{18}\text{O}_{\text{KGW}} + (8 \pm 1)\% \delta^{18}\text{O}_{\text{LP}}$
JC6	-8.2	$\delta^{18}\text{O} = 91\% \delta^{18}\text{O}_{\text{KGW}} + 9\% \delta^{18}\text{O}_{\text{LP}}$
JC8	-8.2	$\delta^{18}\text{O} = (82 \pm 1)\% \delta^{18}\text{O}_{\text{KGW}} + 18\% \delta^{18}\text{O}_{\text{LP}}$
W26	-7.9	$\delta^{18}\text{O} = 91\% \delta^{18}\text{O}_{\text{KGW}} + 9\% \delta^{18}\text{O}_{\text{LP}}$
W25	-8.4	$\delta^{18}\text{O} = 94\% \delta^{18}\text{O}_{\text{KGW}} + 6\% \delta^{18}\text{O}_{\text{LP}}$
W03	-8.3	$\delta^{18}\text{O} = 94\% \delta^{18}\text{O}_{\text{KGW}} + 6\% \delta^{18}\text{O}_{\text{LP}}$
SZ1	-7.5	$\delta^{18}\text{O} = (70 \pm 2)\% \delta^{18}\text{O}_{\text{KGW}} + (30 \pm 2)\% \delta^{18}\text{O}_{\text{LP}}$
SZ2-1	-7.3	$\delta^{18}\text{O} = (63 \pm 1)\% \delta^{18}\text{O}_{\text{KGW}} + (37 \pm 1)\% \delta^{18}\text{O}_{\text{LP}}$
SZ2-2	-7.2	$\delta^{18}\text{O} = (60 \pm 1)\% \delta^{18}\text{O}_{\text{KGW}} + (40 \pm 1)\% \delta^{18}\text{O}_{\text{LP}}$
JC-BR	-7.5	$\delta^{18}\text{O} = (69 \pm 1)\% \delta^{18}\text{O}_{\text{KGW}} + (31 \pm 1)\% \delta^{18}\text{O}_{\text{LP}}$

The results show that the groundwater in the landslide area is mainly supplied by karst water from the adjacent upslope, with proportions ranging from 60% to 94%. Meanwhile, the contribution of local precipitation to the groundwater in the landslide area is relatively small. This suggests that intercepting and redirecting karst water supply from the rear should be the primary focus of any drainage management efforts on the landslide.

Table 4 demonstrates that the contribution of local precipitation to the groundwater at different locations of the landslide varies significantly. JC-BR was sampled at the intersection of drainage borehole JC1 and the horizontal drainage tunnel. The vertically distributed JC1 is located at the rear of the landslide and can discharge the groundwater of the landslide downward, and then through the main tunnel that horizontally penetrates the landslide to discharge the landslide. Due to its good hydraulic conductivity, it is inferred that the drainage channel has a strong ability to receive and collect local precipitation.

Among the groundwater samples collected outside of the artificial drainage facilities, SZ2-1, SZ2-2, and SZ1 exhibit the highest fractions of local precipitation (LP). SZ2 and SZ1 were sampled from the upper sliding surface and the main sliding surface of the landslide, respectively. These results suggest that the sliding rupture surface may provide a continuous pathway for precipitation infiltration and runoff within the landslide, indicating that fissures and fractures in the sliding rupture zone are well connected, which could be a critical factor in the mass movement of the creeping slope.

4. Conclusions

This study aims to investigate the groundwater sources of Huangtupo landslides. By collecting and analyzing groundwater samples, and employing methods such as chemical composition and stable isotopes, the following key conclusions are drawn:

1. Before the relocation of residents from the Huangtupo landslide, the groundwater in the landslide area contained high concentrations of nitrate ions, derived from the direct discharge of domestic sewage onto the slope surface by villagers. As a result, the groundwater of the landslide area was impacted by human sewage, which not only influenced the chemical composition of the groundwater but also had potential implications for slope stability.
2. The primary hydrochemical types in the LGW area are $\text{HCO}_3 \cdot \text{SO}_4 \cdot \text{Ca}$ and $\text{SO}_4 \cdot \text{HCO}_3 \cdot \text{Ca}$. The high concentration of sulfate ions in the landslide groundwater is likely

- derived from gypsum-cemented conglomerates at the top of the Jialingjiang Formation, and the landslide groundwater is recharged by karst water.
3. Stable isotope tracing conducted after the relocation of residents from the Huangtupo landslide confirms that the landslide groundwater originates from a mixture of higher-elevation karst water and local precipitation. The development of conjugate joints in the Badong Formation provides a pathway for the deep migration of karst water. A conceptual flow model reveals the recharge pattern of the landslide groundwater.
 4. The landslide groundwater is a mixture of upslope karst water and landslide precipitation, with karst water being the primary source of recharge. This suggests that intercepting and redirecting the karst water supply from the rear should be the primary focus of any drainage management efforts on the landslide. The groundwater at the sliding rupture surface contains the highest proportion of local precipitation, suggesting that fractures and joints in the rupture zone are interconnected, which could be a critical factor in slope landslide development.
 5. This study lays the theoretical foundation for the stability analysis and drainage management of the Huangtupo landslide and offers valuable insights for investigating the numerous large-scale landslide deposits in the Three Gorges Reservoir area. It is recommended to conduct long-term monitoring and research to enhance our understanding of the landslide groundwater system further and refine the model, ultimately providing more precise evidence for landslide prevention and mitigation.

Author Contributions: Validation, S.C., D.C. and Q.L.; Investigation, S.C. and J.W.; Data curation, S.C. and J.W.; Writing—original draft, S.C.; Writing—review & editing, W.X.; Supervision, W.X.; Project administration, W.X.; Funding acquisition, W.X, J.W., Q.L. and D.C. All authors have read and agreed to the published version of the manuscript.

Funding: The work was funded by the National Natural Science Foundation of China (Nos. 41672297, 41972298 and 42277171) and Hubei Natural Science Foundation of China (Nos. 2022CFB001).

Data Availability Statement: Data is contained within the article.

Acknowledgments: Many thanks to the editors and anonymous reviewers for providing valuable comments that significantly improved this paper.

Conflicts of Interest: The authors declare no conflict of interest.

References

1. Van Asch, T.W.J.; Buma, J.; Van Beek, L.P.H. A view on some hydrological triggering systems in landslides. *Geomorphology* **1999**, *30*, 25–32. [[CrossRef](#)]
2. Iverson, R.M. Landslide triggering by rain infiltration. *Water Resour. Res.* **2000**, *36*, 1897–1910. [[CrossRef](#)]
3. Rutqvist, J.; Stephansson, O. The role of hydromechanical coupling in fractured rock engineering. *Hydrogeol. J.* **2003**, *11*, 7–40. [[CrossRef](#)]
4. Bogaard, T.; Guglielmi, Y.; Marc, V.; Emblanch, C.; Bertrand, C.; Mudry, J. Hydrogeochemistry in landslide research: A review. *Bulletin de la Société Géologique de France* **2007**, *178*, 113–126. [[CrossRef](#)]
5. Vallet, A.; Charlier, J.B.; Fabbri, O.; Bertrand, C.; Carry, N.; Mudry, J. Functioning and precipitation-displacement modelling of rainfall-induced deep-seated landslides subject to creep deformation. *Landslides* **2016**, *13*, 653–670. [[CrossRef](#)]
6. Hua-xi, G.; Kun-long, Y. Study on spatial prediction and time forecast of landslide. *Nat. Hazards* **2014**, *70*, 1735–1748. [[CrossRef](#)]
7. Bogaard, T.A.; Greco, R.; Olivares, L.; Picarelli, L. The Round Robin Test on Landslide Hydrological Modeling at IWL2013. *Procedia Earth Planet. Sci.* **2014**, *9*, 180–188. [[CrossRef](#)]
8. Cappa, F.; Guglielmi, Y.; Soukatchoff, V.M.; Mudry, J.; Bertrand, C.; Charmoille, A. Hydromechanical modeling of a large moving rock slope inferred from slope levelling coupled to spring long-term hydrochemical monitoring: Example of the La Clapière landslide (Southern Alps, France). *J. Hydrol.* **2004**, *291*, 67–90. [[CrossRef](#)]
9. Wang, J.; Su, A.; Xiang, W.; Yeh, H.; Xiong, C.; Zou, Z.; Zhong, C.; Liu, Q. New data and interpretations of the shallow and deep deformation of Huangtupo No. 1 riverside sliding mass during seasonal rainfall and water level fluctuation. *Landslides* **2016**, *13*, 795–804. [[CrossRef](#)]
10. Hua, S. Genetic Mechanism of Multi-Stages Sliding and Evolution Law of the Huangtupo Landslide in the Three Gorges Reservoir Area. Ph.D. Dissertation, China University of Geosciences, Wuhan, China, 2015.
11. Tang, H.; Li, C.; Hu, X.; Su, A.; Wang, L.; Wu, Y.; Criss, R.; Xiong, C.; Li, Y. Evolution characteristics of the Huangtupo landslide based on in situ tunneling and monitoring. *Landslides* **2015**, *12*, 511–521. [[CrossRef](#)]

12. Wang, J.; Xiang, W.; Lu, N. Landsliding triggered by reservoir operation: A general conceptual model with a case study at Three Gorges Reservoir. *Acta Geotech.* **2014**, *9*, 771–788. [[CrossRef](#)]
13. Deng, Q.L. *Slope Tectonics: An Example Analysis of the New County-Seat Town Slope of Badong*; China University of Geosciences Press: Wuhan, China, 2000.
14. Dong, Y.; Liao, Z.; Wang, J.; Liu, Q.; Cui, L. Potential failure patterns of a large landslide complex in the Three Gorges Reservoir area. *Bull. Eng. Geol. Environ.* **2023**, *82*, 41. [[CrossRef](#)]
15. Guglielmi, Y.; Bertrand, C.; Compagnon, F.; Follacci, J.P.; Mudry, J. Acquisition of water chemistry in a mobile fissured basement massif: Its role in the hydrogeological knowledge of the La Clapière landslide (Mercantour massif, southern Alps, France). *J. Hydrol.* **2000**, *229*, 138–148. [[CrossRef](#)]
16. Guglielmi, Y.; Cappa, F.; Amitrano, D. High-definition analysis of fluid-induced seismicity related to the mesoscale hydromechanical properties of a fault zone. *Geophys. Res. Lett.* **2008**, *35*, L06306. [[CrossRef](#)]
17. Cervi, F.; Ronchetti, F.; Martinelli, G.; Bogaard, T.A.; Corsini, A. Origin and assessment of deep groundwater inflow in the Ca’Lita landslide using hydrochemistry and in situ monitoring. *Hydrol. Earth Syst. Sci.* **2012**, *16*, 4205–4221. [[CrossRef](#)]
18. Cervi, F.; Corsini, A.; Doveri, M.; Mussi, M.; Ronchetti, F.; Tazioli, A. Characterizing the Recharge of Fractured Aquifers: A Case Study in a Flysch Rock Mass of the Northern Apennines (Italy). In Proceedings of the IAEG XII Congress: Engineering Geology for Society and Territory, Torino, Italy, 13–19 September 2014; pp. 563–567.
19. Dansgaard, W. Stable isotopes in precipitation. *Tellus* **1964**, *16*, 436–468. [[CrossRef](#)]
20. McCarthy, K.A.; McFarland, W.D.; Wilkinson, J.M.; White, L.D. The dynamic relationship between ground water and the Columbia River: Using deuterium and oxygen-18 as tracers. *J. Hydrol.* **1992**, *135*, 1–12. [[CrossRef](#)]
21. Peng, T.; Wang, C.; Lai, T.; Ho, F.S. Using hydrogen, oxygen, and tritium isotopes to identify the hydrological factors contributing to landslides in a mountainous area, central Taiwan. *Environ. Geol.* **2007**, *52*, 1617–1629. [[CrossRef](#)]
22. Peters, E.; Visser, A.; Esser, B.; Moran, J. Tracers Reveal Recharge Elevations, Groundwater Flow Paths and Travel Times on Mount Shasta, California. *Water* **2018**, *10*, 97. [[CrossRef](#)]
23. Gao, M.; Li, X.; Qian, J.; Wang, Z.; Hou, X.; Fu, C.; Ma, J.; Zhang, C.; Li, J. Hydrogeochemical Characteristics and Evolution of Karst Groundwater in Heilongdong Spring Basin, Northern China. *Water* **2023**, *15*, 726. [[CrossRef](#)]
24. Compagnon, F.; Guglielmi, Y.; Mudry, J.; Follacci, J.; Ivaldi, J. Approche chimique et isotopique de l’origine des eaux en transit dans un grand mouvement de terrain: Exemple du glissement de La Clapière (Alpes-Maritimes, France). *Comptes Rendus De l’Académie Des Sci.-Ser. IIA-Earth Planet. Sci.* **1997**, *325*, 565–570. [[CrossRef](#)]
25. Peng, T.; Wang, C.; Hsu, S.; Wang, G.; Su, T.; Lee, J. Identification of groundwater sources of a local-scale creep slope: Using environmental stable isotopes as tracers. *J. Hydrol.* **2010**, *381*, 151–157. [[CrossRef](#)]
26. Mebrahtu, T.K.; Banning, A.; Girmay, E.H.; Wohnlich, S. The effect of hydrogeological and hydrochemical dynamics on landslide triggering in the central highlands of Ethiopia. *Hydrogeol. J.* **2021**, *29*, 1239–1260. [[CrossRef](#)]
27. Binet, S.; Jomard, H.; Lebourg, T.; Guglielmi, Y.; Tric, E.; Bertrand, C.; Mudry, J. Experimental analysis of groundwater flow through a landslide slip surface using natural and artificial water chemical tracers. *Hydrol. Process.* **2007**, *21*, 3463–3472. [[CrossRef](#)]
28. Charlier, J.; Bertrand, C.; Binet, S.; Mudry, J.; Bouillier, N. Use of continuous measurements of dissolved organic matter fluorescence in groundwater to characterize fast infiltration through an unstable fractured hillslope (Valabres rockfall, French Alps). *Hydrogeol. J.* **2010**, *18*, 1963–1969. [[CrossRef](#)]
29. Vallet, A.; Bertrand, C.; Mudry, J.; Bogaard, T.; Fabbri, O.; Baudement, C.; Régent, B. Contribution of time-related environmental tracing combined with tracer tests for characterization of a groundwater conceptual model: A case study at the Séchilienne landslide, western Alps (France). *Hydrogeol. J.* **2015**, *23*, 1761–1779. [[CrossRef](#)]
30. Deng, Q.L.; Zhu, Z.Y.; Cui, Z.Q.; Wang, X.P. Mass rock creep and landsliding on the Huangtupo slope in the reservoir area of the Three Gorges Project, Yangtze River, China. *Eng. Geol.* **2000**, *58*, 67–83. [[CrossRef](#)]
31. Wu, S.; Shi, L.; Wang, R.; Tan, C.; Hu, D.; Mei, Y.; Xu, R. Zonation of the landslide hazards in the forereservoir region of the Three Gorges Project on the Yangtze River. *Eng. Geol.* **2001**, *59*, 51–58. [[CrossRef](#)]
32. Di Maio, C.; Vassallo, R.; Vallario, M.; Pascale, S.; Sdao, F. Structure and kinematics of a landslide in a complex clayey formation of the Italian Southern Apennines. *Eng. Geol.* **2010**, *116*, 311–322. [[CrossRef](#)]
33. Huang, F.; Luo, X.; Liu, W. Stability Analysis of Hydrodynamic Pressure Landslides with Different Permeability Coefficients Affected by Reservoir Water Level Fluctuations and Rainstorms. *Water* **2017**, *9*, 450. [[CrossRef](#)]
34. Van der Spek, J.E.; Bogaard, T.A.; Bakker, M. Characterization of groundwater dynamics in landslides in varved clays. *Hydrol. Earth Syst. Sci.* **2013**, *17*, 2171–2183. [[CrossRef](#)]
35. Jiang, J. Research on the Deformation Mechanism and Dynamic Response of Typical Landslides in Three Gorges Reservoir in Case of Frequent Microseisms. Ph.D. Dissertation, China University of Geosciences, Wuhan, China, 2012.
36. Craig, H. Isotopic Variations in Meteoric Waters. *Science* **1961**, *133*, 1702–1703. [[CrossRef](#)] [[PubMed](#)]
37. Zheng, S.; Hou, F.; Ni, B.; Adler, M. Study on Hydrogen and oxygen stable isotopes of atmospheric precipitation in China. *Sci. Bull.* **1983**, *28*, 801.
38. Huang, H.; Luo, M.; Chen, Z.; Zhou, H.; Zhang, L. The spatial and temporal distribution of stable hydrogen and oxygen isotope of meteoric water in Xiangxi river basin. *Hydrogeol. Eng. Geol.* **2016**, *43*, 36–42. [[CrossRef](#)]
39. Yu, J.; Zhang, H.; Yu, F.; Liu, D. Oxygen isotopic composition of meteoric water in the eastern part of Xizang. *Geochimica* **1980**, *01*, 113–121. [[CrossRef](#)]

40. Yu, J.; Yu, F.; Liu, D. The oxygen and hydrogen isotopic compositions of meteoric waters in the eastern part of China. *Geochimica* **1987**, *1*, 22–26. [[CrossRef](#)]
41. Criss, R.; Fernandes, S.; Winston, W. Isotopic, Geochemical and Biological Tracing of the Source of an Impacted Karst Spring, Weldon Spring, Missouri. *Environ. Forensics* **2001**, *2*, 99–103. [[CrossRef](#)]

Disclaimer/Publisher’s Note: The statements, opinions and data contained in all publications are solely those of the individual author(s) and contributor(s) and not of MDPI and/or the editor(s). MDPI and/or the editor(s) disclaim responsibility for any injury to people or property resulting from any ideas, methods, instructions or products referred to in the content.